A&A 423, L29–L32 (2004)
DOI: 10.1051/0004-6361:200400029

Astronomy & Astrophysics

Letter to the Editor

Interstellar turbulence driven by the magnetorotational instability

N. Dziourkevitch, D. Elstner, and G. Rüdiger

Astrophysikalisches Institut Potsdam, An der Sternwarte 16, 14482 Potsdam, Germany
e-mail: nsdziourkevitch@aip.de

Received 26 March 2004 / Accepted 5 July 2004

Abstract. The occurrence of the magnetorotational instability (MRI) in vertically stratified galactic disks is considered. Global 3D nonlinear MHD simulations with the ZEUSMP code are performed in a cylindric computational domain. Due to the evolution of the MRI toroidal and poloidal components of the mean magnetic fields are generated. The results are also applied to very young galaxies which are assumed to possess strong magnetic fields already after a few 10^8 years. The dependence of MRI growth rate on the shear strength is shown. The velocity dispersion grows with height and reaches values of about 5 km s^{-1} in good agreement with observations and close to the predictions of Sellwood & Balbus (1999). For strong magnetic fields the MRI is suppressed but it is not suppressed by turbulence initially present in the disk.

Key words. MHD – galaxies: magnetic fields – galaxies: evolution

1. Introduction

Radio observations of polarized synchrotron emission show the existence of large scale magnetic fields in nearby spiral galaxies which is mainly axisymmetric and of quadrupolar equatorial parity (Beck 2000). The standard dynamo theory explains both symmetries but it has difficulties to produce the fields fast enough. Also the field strength of several μG can reasonably be explained with the concept of the turbulent $\alpha^2\Omega$-dynamo. The question remains, however, about the seed field for the dynamo, which should already have a large scale quadrupolar part. The battery effect cannot yield a seed field with such a parity (Krause & Beck 1998).

Supernovae explosions and stellar winds are often considered to maintain the interstellar turbulence. The magnetorotational instability (MRI), however, provides another source of turbulence. In a differentially rotating disk with outwards decreasing angular velocity the instability requires only the presence of a weak magnetic field, orders of magnitude below the observed field strength of a few μG. There are several arguments in favor of the MRI rather than the SN-explosion concept:

(i) In the Milky Way line widths of individual molecular and HI clouds and cloud complexes exceed the expected thermal width compared to estimated kinematic temperatures. The 21 cm dispersion does not drop below 5–7 km s^{-1}, regardless of how low the optical surface brightness becomes. Obviously, interstellar turbulence does not decay in regions without star formation activity. A theoretical investigations of MRI-driven turbulence acting in a disk was applied to the particular case of NGC 1058, a face-on disk galaxy with a well-studied extended HI disk (Sellwood & Balbus 1999). This implied a magnetic field of about 3 μG which well agrees with the observed field value of many galaxies.

(ii) Some flocculent galaxies may possess regular magnetic fields with a strong radial component as in NGC 4414 (Soida et al. 2002). The velocity field shows no evidence for spiral waves. NGC 4414 has a high surface density and is forming stars fairly intensively, like in the Milky Way, but it is in no way a starburst galaxy.

(iii) Magnetic fields are observed in extremely young galaxies (Kronberg et al. 1992; Lesch & Hanasz 2003). The magnetic fields are required to be amplified strongly on short time-scales ($\gtrsim 10^7$ yr), because of the observed magnetization of very young (0.5 Gyr) galaxies.

MRI is present if a disk is differentially rotating with a rate decreasing with distance from the center and has a weak (magnetic Mach number <1) poloidal magnetic field component. Kitchatinov & Rüdiger (2004) worked for their linear but global analysis with a large magnetic Prandtl number Pm up to 10^4 due to the high values of the microscopic viscosity. As the real value of Pm for galaxies is much higher ($\nu \sim 10^{18}$ cm^2 s^{-1}, $\eta \sim 10^7$ cm^2 s^{-1}) the results can only be used as the basis for a scaling procedure. The linear analysis of MRI-generated magnetic field disturbances shows an exponential growth $B \sim \exp(\gamma t)$ with the growth rate $\gamma \simeq \tau_{\rm rot}^{-1}$, where $\tau_{\rm rot} = 2\pi/\Omega_0$ is a rotation time at the transition radius to differential rotation. The result was derived for Brandt-type rotation law (Eq. (4), Sect. 2) with $n = 2$. As an example, for a rotation time of 70 Myr (NGC 6946, Sofue 1996) MRI can amplify a seed field of 10^{-12} G to the observed value of 10^{-6} G during 1 Gyr. Notice that the local analysis predicts $\gamma = 0.5q\Omega_0$ with normalized shear $q = -(R/\Omega_0)\partial\Omega/\partial R$. Since the Ω_0 is 75 Gyr^{-1} and 100 Gyr^{-1}

for models 2 and 3 (Sect. 3.2) with the $q_{\max} = 0.4$, it is clear that the local growth rates would be 15 Gyr^{-1} and 20 Gyr^{-1} respectively. The corresponding e-folding times are 67 and 50 Myr. It will be shown in Sect. 3.2 that e-folding times are larger in the global case.

Our 3D nonlinear simulations provide the occurrence of velocity flows and magnetic fields variations due to MRI for models both with uniform density and with stratified density, confirming the predictions of global linear investigations and extending them into the nonlinear domain.

2. The model

The MHD equations

$$\rho\frac{\mathrm{d}\boldsymbol{u}}{\mathrm{d}t} = -\nabla P - \rho\nabla\Psi + \frac{1}{\mu_0}(\nabla\times\boldsymbol{B})\times\boldsymbol{B}, \quad (1)$$

$$\frac{\partial\boldsymbol{B}}{\partial t} = \nabla\times(\boldsymbol{u}\times\boldsymbol{B}) \quad (2)$$

and

$$\frac{\partial\rho}{\partial t} + \nabla\cdot(\rho\boldsymbol{u}) = 0 \quad (3)$$

are solved with the help of the 3D ZEUSMP code using uniform grids. The feedback of magnetic fields $\boldsymbol{B}$ onto the velocity field $\boldsymbol{u}$ is included as a Lorentz force in the Navier-Stokes equation. The isothermal relation $P = c_{\mathrm{ac}}^2\rho$ with the sound speed $c_{\mathrm{ac}} = 10$ km s^{-1} is used for the interstellar medium.

The resolution is chosen to be from 8 to 11 grid points for resolving the minimal wavelength, its initial value was calculated according to Balbus & Hawley (1991a,b). Only numerical diffusivities are included. Artificial viscosity is introduced in every model. It dissipates high-frequency numerical noise and smears out shock fronts if the flow becomes supersonic.

3D global calculations in the cylindrical coordinates have been done for a disk of thickness $z = [-1, 1]$ kpc and $R = [1, 5]$ kpc. The gravitation potential Ψ is assumed to be generated by the stellar population, self-gravity of the gas is not included. We have prescribed the potential Ψ for radial and vertical directions separately so that similar shape in stratification and rotation curve profile result following Fröhlich & Schultz (1996). No azimuthal variations like density waves and spirals are introduced. All non-axisymmetric structures in density or flow and fields in the simulations are thus due to MRI. The rotation curve

$$u_\phi = \frac{R\,\Omega_0}{(1+(R/R_0)^n)^{1/n}} \quad (4)$$

is the Brandt-type law. We assume $n = 2$ for all models. The initial magnetic fields are chosen to be vertical and homogeneous everywhere in the disk. Radial boundaries are set to perfect conductor. In vertical direction we have chosen pseudo-vacuum boundary conditions. No supernova-driven turbulence is taken into account, only very small random density perturbations are assumed as the initial condition.

The disk proves to be stable for rigid rotation but also without magnetic fields. For too high initial vertical fields ($B_0 \geq 7\ \mu$G, i.e. $V_{\mathrm{A},0} \geq 20$ km s^{-1}) the disk becomes also stable.

Table 1. Models with homogeneous density ($\rho_0 = 0.47\times10^{-24}$ g/cm^3).

B [μG]	$V_{\mathrm{A},0}$ [km s^{-1}]	λ_z [pc]	u_{T} [km s^{-1}]	B_{T} [μG]	$V_{\mathrm{A,T}}$ [km s^{-1}]
0.11	0.45	130	2.3	1.0	4.1
0.22	0.9	220	8.3	2.3	9.4
0.44	1.8	400	17	4.3	17.6
0.66	2.7	616	22	4.7	19.3

Table 2. Density-stratified models with different rotation laws.

Model	R_0 [kpc]	Ω_0 [Gyr^{-1}]	B_0 [μG]	u_{T} [km s^{-1}]	B_{T} [μG]	$V_{\mathrm{A,T}}$ [km s^{-1}]
1	2.3	75	0.11	2.7	0.4	9
2	2.3	75	0.32	5.8	1.4	24
3	2.0	100	0.32	7.8	2.0	43

3. Results

3.1. Uniform density

In Table 1 the runs with identical rotation curves but for different magnetic field amplitudes are presented. For magnetic fields B the corresponding Alfvén velocity is $V_{\mathrm{A}} = B/\sqrt{\mu_0\rho}$. One finds that the typical wavelength λ_z grows linearly with the initial magnetic field. This is a well known result of the linear theory (Velikhov 1959; Fricke 1969; Balbus & Hawley 1991a). Another two runs with initial Alfvén velocities $V_{\mathrm{A}} = 1.8$ km s^{-1} and $V_{\mathrm{A}} = 2.7$ km s^{-1} were done in addition to confirm the linear theory prediction. For seed field of 10^{-12} G one can estimate the typical MRI wavelength $\lambda_z \lesssim 10^{-3}$ pc. But the wavelength should increase with the increasing magnetic field, what we observed also in our simulations. The upper limit for initial magnetic fields for MRI will be the value when the corresponding wavelength of instability will exceed the doubled disk thickness. Our tests show that MRI is cut off if initial magnetic field is about 7 μG.

Also the characteristic kinetic velocity $u_{\mathrm{T}} = (\langle u_R'^2\rangle + \langle u_\phi'^2\rangle)^{1/2}$ grows with the applied magnetic field. For the given examples it reaches values of a few km s^{-1} while the small-scale magnetic fluctuation $B_{\mathrm{T}} = (\langle B_R'^2\rangle + \langle B_\phi'^2\rangle)^{1/2}$ is order of a few μG. Its Alfvén velocity exceeds the Alfvén velocity of the external field by a factor of 10 but its value is close to u_{T} so that roughly equipartition results ($V_{\mathrm{A,T}} \simeq u_{\mathrm{T}}$).

3.2. Nonuniform density

The model can be improved by adopting the density stratification

$$\rho = \sum_m \rho_{0,m}\exp\left(-\frac{z^2}{H_m^2}\right) \quad (5)$$

with $\rho_0 = 10^{-24}$ g/cm^3 (Dickey & Lockman 1990). The initial magnetic field which we used are given in Table 2 and also the rotation curves have been varied.

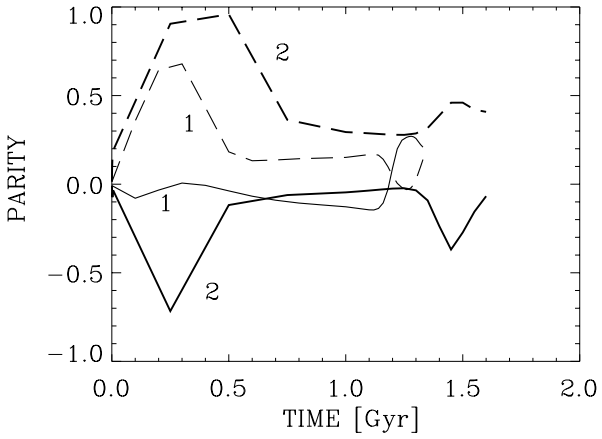

Fig. 1. The magnetic parity P of the axisymmetric components of the magnetic fields of models 1 and 2 of Table 2 (solid). Dipoles and quadrupoles seem to balance. The parity of the axisymmetric components of the flow (dashed). The existence of mixed modes is indicated for both field and flow.

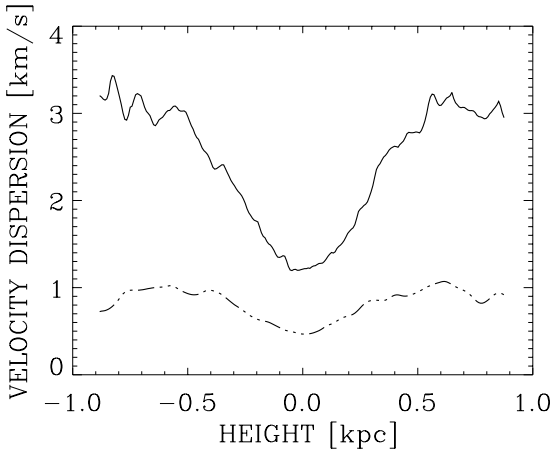

Fig. 2. The turbulent intensity u_T for model 1 has a minimum at the disk midplane after 1.33 Gyr. The same holds for u_z (dashed).

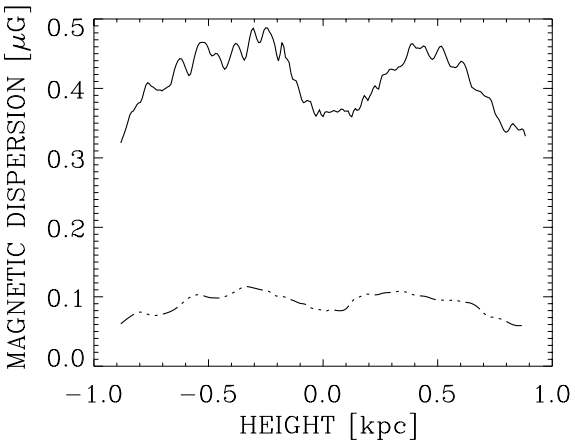

Fig. 3. The same as in Fig. 2 but for the magnetic dispersion B_T which also has a minimum at the midplane. The dashed line gives B_z.

The results are summarized in the Table 2. Model 1 works with a weak magnetic field which is increased in the models 2 and 3 which differ by the rotation laws. The turbulence intensity slightly exceeds the value 5 km s^{-1}. The characteristic amplitude of the magnetic field fluctuations is about 1 μG or – expressed as Alfvén velocity more than 20 km s^{-1}. The values are the higher the stronger the differential rotation is (compare models 2 and 3). Comparison of stability diagrams for the dipolar and quadrupole magnetic patterns from the linear global model of Kitchatinov & Rüdiger (2004) shows that the quadrupolar solution has a bit wider branches. It means that this symmetry has smaller minimum magnetic fields for being excited and it needs larger maximum fields for instability termination. The parity P is defined with

$$P = \frac{E^{\rm Q} - E^{\rm D}}{E^{\rm D} + E^{\rm Q}} \qquad (6)$$

where $E^{\rm D}$ ($E^{\rm Q}$) is the energy of the modes with dipolar (quadrupolar) symmetry. So one would expect the mixed parity to appear in nonlinear regime.

The value of parity (6) is −1 for a strict dipolar field structure and it is +1 for quadrupole. Figure 1 gives the results for the symmetries of the magnetic field. As the initial field B_0 is antisymmetric with respect to the midplane the magnetic fields parity starts in all cases with stronger dipolar part but it approaches zero after a few rotations. Indeed, the final solution due to MRI is a mixed mode. Figures 2 and 3 present the vertical profiles of the turbulent flow and field intensities. Both the flow and the field fluctuations show a minimum at the equator. This result well complies with the observation of strong turbulence in the galactic halos (Pietz et al. 1998; Kalberla et al. 1998; see Fletcher & Shukurov 2001) and with the computations by Fröhlich & Schultz (1996). It is opposite to the situation which one expects if the interstellar turbulence would be driven by SN-explosions (Ferrière 1992; Kaisig et al. 1993; Ziegler 1996; Korpi et al. 1999).

Figure 4 shows the magnetic vectors overplotted on the contour of density fluctuations. The face-on slide is taken as an equatorial cut of simulated gaseous galactic disk. Fluctuations of density in radial direction are not great, about 50% from the initial value (no radial or azimuthal dependence of density was prescribed). As one can see, the instability works only in the region of $R > R_0$, i.e. in the region of non-zero shear. Inside the ring with the radius $R < 2$ kpc no radial or azimuthal magnetic fields components are generated. Dark-shades regions are the minimums of density, maximums of magnetic fields are correlating with dark-shades regions. The plot was made after a local averaging procedure. One can see close-spiral or almost ring structure created by MRI, after the cells were stretched along the azimuth during rotations. Magnetic pitch angles are about −30°, and the mean magnetic fields have mixed symmetry in respect to the galactic plane. The magnetic field is found to grow exponentially with the e-folding time T [Myr] depending directly on the rotation time $\tau_{\rm rot} = 2\pi/\Omega_0$. The instability is very fast in our simulations: its e-folding time is only 60−86 Myr depending on the strength of the rotation (Table 3). E-folding time of the magnetic field T suits to the global linear analysis prediction $T \simeq \tau_{\rm rot}$ ($\tau_{\rm rot}$ is 84 Myr for model 2 and 63 Myr for model 3 in Table 2). These times are longer then the local theory predictions (Sect. 1). The explanation is a decrease of the shear absolute value from 0.4 to 0.3 with the

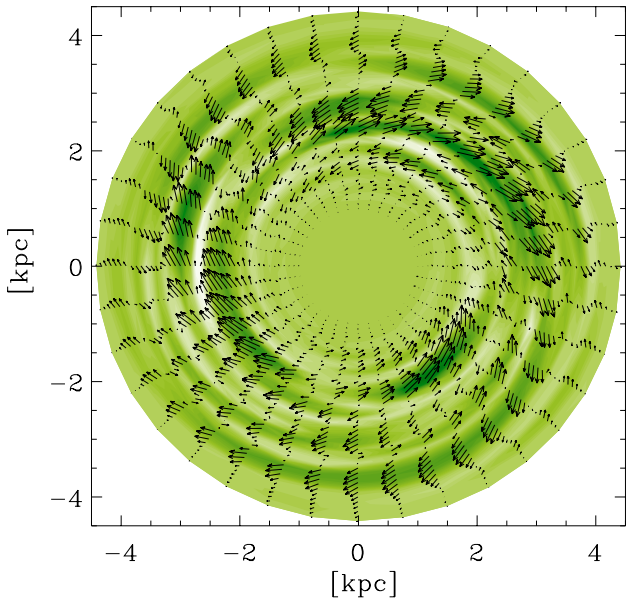

Fig. 4. Model 3: the density minima are shown in dark-green (or dark shadows), overplotted are the arrows of the magnetic field.

Table 3. Simulations results e-folding time of magnetic field T and the ratio of kinetic to magnetic energy for the models 2 and 3. In the last column the ratio Maxwell to Reynolds stress is given.

Model	T [Myr]	$E_{\rm kin}/E_{\rm mag}$	MS/RS
2	86	3.8	120
3	60	3.5	452

radius. Notice, that the magnetic field in model 3 will be amplified by factor of 10^6 per Gyr in the global model, whereas the local prediction is an amplification by factor of 10^8 per Gyr.

The instability is magnetic-dominated: the magnetic energy exceeds the kinetic energy by a factor of 4. More dramatic is the situation concerning the angular momentum transport. The Reynolds stress is small and less than 1% of the Maxwell stress. The angular momentum transport is thus completely dominated by the magnetic field fluctuations.

4. Conclusions

Our nonlinear 3D MHD simulations lead to expected and unexpected aspects of the global action of MRI. The typical wavelength of the instability is proportional to the initial magnetic field strength. The model reproduces the observed rms values of magnetic fields and velocity in the interstellar turbulence. We have also confirmed the prediction of Sellwood & Balbus (1999) that the turbulent velocity dispersion is linked to the Alfvén speed.

Another important property of the MRI-driven turbulence is that the dispersion grows outside of the disk plane while SN-driven turbulence found to be concentrated within the disk. The velocity turbulence increasing outwards is quite important to decide the question how the galactic dynamo is driven. Similar effect has previously been described by saying that the stress is not proportional to density (Brandenburg et al. 1996). Comparing Figs. 3, 4 and stress vertical dependence in work of Brandenburg et al. (1996) one can see that turbulent parameters are increasing with heights by factor of about 2−3 but not by factor of 30 as density drops.

The MRI is also shown to be a very fast instability with e-folding time of $\tau_{\rm rot} = 2\pi/\Omega_0$. Therefore, MRI easily could explain the existence of rather large magnetic fields in very young galaxies. As we have also shown with the simulations that the dispersion of about 5 km s^{-1} is quite a normal number for shear instability in galaxies.

The resulting turbulence pattern both exhibits spiral or more ring-like structures but the Maxwell stress $B_R^{'} \cdot B_\phi^{'}$ is always negative, so that the angular momentum is always transported outwards. The magnetic fields have many reversals between the rings but averaged pitch angle is always negative with an amplitude of about −30°.

References

Balbus, S. A., & Hawley, J. F. 1991a, ApJ, 376, 214
Balbus, S. A., & Hawley, J. F. 1991b, ApJ, 376, 223
Brandenburg, A., Nordlund, Å, Stein, R. F., & Torkelsson, U. 1996, Physics of Accretion Disks, ed. S. Kato, S. Inagaki, S. Mineshige, & J. Fukue (Gordon and Breach Science Publishers), 285
Beck, R. 2000, Phil. Trans. R. Soc. Lond. A, 358, 777
Caselli, P., Meyers, P. C., & Thaddeus, P. 1995, ApJ, 455, L77
Dickey, J. M., Hanson, M. M., & Helou, G. 1990, ApJ, 352, 522
Dickey, J. M., & Lockman, F. J. 1990, ARA&A, 28, 215
Drecker, A., Rüdiger, G., & Hollerbach, R. 2000, MNRAS, 317, 45
Ferrière, K. 1992, ApJ, 389, 286
Fletcher, A., & Shukurov, A. 2001, MNRAS, 325, 312
Fricke, K. 1969, A&A, 1, 388
Fröhlich, H.-E., & Schultz, M. 1996, A&A, 311, 451
Haugen, N. E. L., Brandenburg, A., & Dobler, W. 2003, ApJ, 597, L141
Kaisig, M., Rüdiger, G., & Yorke, H. W. 1993, A&A, 274, 757
Kalberla, P. M. W., Westphalen, G., Mebold, U., et al. 1998, A&A, 332, L61
Kitchatinov, L., & Rüdiger, G. 2004 [arXiv:astro-ph/0405228]
Korpi, M. J., Brandenburg, A., Shukurov, A., et al. 1999, ApJ, 514, L99
Krause, F., & Beck, R. 1998, A&A, 335, 789
Kronberg, P. P., Perry, J. J., & Zukowski, E. L. 1992, ApJ, 387, 528
Lesch, H., & Hanasz, M. 2003, A&A, 401, 809
Miesch, M. S., & Bally, J. 1994, ApJ, 429, 645
Pietz, J., Kerp, J., Kalberla, P. M. W., et al. 1998, A&A, 332, 55
Sellwood, J. A., & Balbus, S. A. 1999, ApJ, 511, 660
Sofue, Y. 1996, ApJ, 458, 120
Soida, M., Beck, R., Urbanik, M., & Braine, J. 2002, A&A, 394, 47
Velikhov, E. 1959, Sov. Phys. JETP, 9, 995
Zeigler, U. 1996, A&A, 313, 448